New Journal of Physics
The open access journal for physics

Broadband excitation by chirped pulses: application to single electron spins in diamond

I Niemeyer[1], J H Shim[1], J Zhang[1], D Suter[1,6], T Taniguchi[2], T Teraji[2], H Abe[3], S Onoda[3], T Yamamoto[3], T Ohshima[3], J Isoya[4] and F Jelezko[5]

[1] Fakultät Physik, Technische Universität Dortmund, Dortmund, Germany
[2] National Institute for Materials Science, 1-1 Namiki, Tsukuba, Ibaraki 305-0044, Japan
[3] Japan Atomic Energy Agency, 1233 Watanuki, Takasaki, Gunma 370-1292, Japan
[4] Research Center for Knowledge Communities, University of Tsukuba, Tsukuba 305-8550, Japan
[5] Institut für Quantenoptik, Universität Ulm, Ulm, Germany
E-mail: Dieter.Suter@tu-dortmund.de

New Journal of Physics **15** (2013) 033027 (14pp)
Received 7 December 2012
Published 21 March 2013
Online at http://www.njp.org/
doi:10.1088/1367-2630/15/3/033027

Abstract. Pulsed excitation of broad spectra requires very high field strengths if monochromatic pulses are used. If the corresponding high power is not available or not desirable, the pulses can be replaced by suitable low-power pulses that distribute the power over a wider bandwidth. As a simple case, we use microwave pulses with a linear frequency chirp. We use these pulses to excite spectra of single nitrogen–vacancy centres in a Ramsey experiment. Compared to the conventional Ramsey experiment, our approach increases the bandwidth by at least an order of magnitude. Compared to the conventional continuous wave-ODMR experiment, the chirped Ramsey experiment does not suffer from power broadening and increases the resolution by at least an order of magnitude. As an additional benefit, the chirped Ramsey spectrum contains

[6] Author to whom any correspondence should be addressed.

not only 'allowed' single quantum transitions, but also 'forbidden' zero- and double quantum transitions, which can be distinguished from the single quantum transitions by phase-shifting the readout pulse with respect to the excitation pulse or by variation of the external magnetic field strength.

Contents

1. Introduction **2**
2. Mathematical descriptions **3**
2.1. Spin $S = 1/2$ system . . . 3
2.2. Spin $S = 1$ system . . . 4
2.3. Adiabatic condition . . . 6
3. Experimental results **7**
3.1. Setup and samples . . . 7
3.2. Phase shifts . . . 8
3.3. B-field dependence . . . 10
3.4. Multi-line broadband spectrum . . . 11
4. Conclusions **13**
Acknowledgments **13**
References **13**

1. Introduction

Nitrogen–vacancy (NV) defect centres in diamond are promising candidates for quantum information processing [1], magnetometry [2–4] and electrometry [5]. The recently measured temperature dependence of the zero-field splitting constant [6, 7] indicates that it may also be used as an atomic temperature sensor. Even very weakly coupled nuclear spins can be detected by using appropriate pulse sequences [8–10]. The centre consists of a substitutional nitrogen atom adjacent to a vacancy in the diamond crystal lattice. In the negatively charged state, it has an electron spin $S = 1$. Excitation with green laser light polarizes the spin at room temperature $\approx$90% [1] into the $|m_s = 0\rangle$ ground state. This state (usually denoted as 'bright state') exhibits a higher fluorescence rate than the $|m_s = \pm 1\rangle$ spin levels. Microwave pulses can transfer population between the $|m_s = 0\rangle \leftrightarrow |m_s = \pm 1\rangle$ spin levels. The populations can be measured via the photon scattering rate [1].

Quantum computing with NV-centres can not only use the electron spin, but also hybrid quantum registers with additional nuclear spins. In particular, strongly coupled ^{13}C nuclear spins have attractive properties [11–15]. The strength of the hyperfine interaction depends on the position of the nuclear spin [15, 16] and reaches a maximum of 130 MHz for a ^{13}C in a nearest-neighbour lattice site [1, 17]. Measuring these couplings requires the recording of spectra that cover a frequency range larger than the sum of all hyperfine coupling constants. This can be done by continuous wave (CW)-ODMR, which yields spectra with linewidths of several MHz under typical conditions. These linewidths are the result of power broadening by the laser and the microwave field. The effect of the laser is eliminated in the pulsed ODMR approach [15, 18], where the laser is switched off during the application of the microwave field. The remaining broadening from the microwave field is also eliminated in the Ramsey experiments [19, 20],

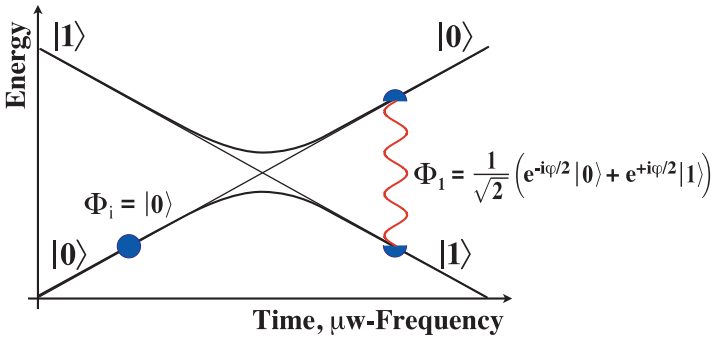

Figure 1. Excitation of a two-level system by non-adiabatic rapid passage. For an adiabatic passage the initial and final states of the system are equal to the non-perturbed eigenstate ($|0\rangle$, $|1\rangle$). After a non-adiabatic passage, the final state is a coherent superposition of the eigenstates $|0\rangle$ and $|1\rangle$. The conditions for the adiabaticity of a passage are discussed in section 2.3.

which yields spectra with linewidths equal to the natural linewidth. The drawback of the Ramsey experiment is that it requires excitation pulses that cover the full bandwidth of the spectrum. This can be challenging for spectra with large hyperfine couplings.

Here, we present an experimental scheme that avoids power broadening by using the Ramsey approach of free precession and the requirement of strong microwave fields by using excitation pulses that cover the full bandwidth with very low power. Compared to the pulsed ODMR approach, this method does not suffer from a trade-off between signal intensity and resolution. We achieve this by scanning the frequency over the full spectral range. This type of pulses are known as chirped pulses [21–23].

Since the microwave field interacts with the different transitions sequentially, it excites not only the usual, magnetic-dipole allowed transitions between the $|m_S = 0\rangle \leftrightarrow |m_S = \pm 1\rangle$ states (single quantum transitions), but also the 'forbidden' transition between the $|m_S = -1\rangle \leftrightarrow |m_S = +1\rangle$ states (double quantum transition). These different types of transitions can be distinguished by appropriate shifts in the relative phases of the excitation and readout pulses.

2. Mathematical descriptions

2.1. Spin $S = 1/2$ system

We use chirped excitation pulses to excite transitions in a large frequency range. Figure 1 shows the basic idea: assuming that we want to excite the transition between the $|m_S = 0\rangle$ and the $|m_S = 1\rangle$ state and that the system is initially in the ground state, we scan the frequency through resonance in such a way that the system has a 50% transition probability to the $|m_S = 1\rangle$ state and ends up in the superposition state

$$\Phi_1 = \frac{1}{\sqrt{2}}\left(e^{-i\varphi_1/2}|0\rangle + e^{i\varphi_1/2}|1\rangle\right),$$

which maximizes the coherence between the two levels. To reach this state, the sweep must be non-adiabatic. The conditions for this are discussed in section 2.3. The relative phase φ depends on the phase, amplitude and scan rate of the microwave.

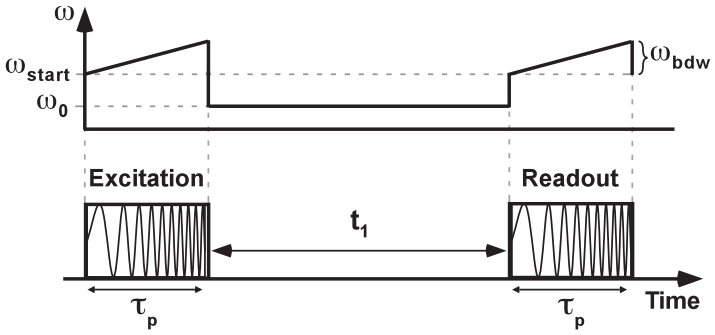

Figure 2. Pulse sequence for broadband Ramsey experiment with chirped excitation pulses. ω_{start} defines the start frequency of the scan and ω_{bdw} the width of the scan. ω_0 is the reference frequency that relates the phase of the two pulses; for details see text. τ_{p} is the pulse duration and t_1 the free evolution time which is incremented between experiments.

The effect of the chirped pulse can thus be described by a unitary operator [23]

$$U_{zy}\left(\varphi_1, \frac{\pi}{2}\right) = \mathrm{e}^{-\mathrm{i}\varphi_1 S_z}\, \mathrm{e}^{-\mathrm{i}\frac{\pi}{2} S_y}.$$

As shown in figure 2, the system is then allowed to evolve freely for a time t_1. If Ω_0 is the Larmor frequency of the system, the superposition state acquires an additional phase $\Omega_0 t_1$ during this time. The resulting state is

$$\begin{aligned}\Phi_2 &= \mathrm{e}^{-\mathrm{i}\Omega_0 t_1 S_z}\Phi_1 \\ &= \frac{1}{\sqrt{2}}\left(\mathrm{e}^{-\mathrm{i}(\Omega_0 t_1+\varphi_1)/2}|0\rangle + \mathrm{e}^{\mathrm{i}(\Omega_0 t_1+\varphi_1)/2}|1\rangle\right).\end{aligned}$$

At this point, a second chirped pulse generates another transformation that we write as

$$U_{yz}\left(\frac{\pi}{2}, \varphi_2\right) = \mathrm{e}^{-\mathrm{i}\frac{\pi}{2} S_y}\, \mathrm{e}^{-\mathrm{i}\varphi_2 S_z},$$

thus converting the system into the final state

$$\Phi_3 = \mathrm{i}\sin\left(\frac{\Omega_0 t_1+\varphi_1+\varphi_2}{2}\right)|0\rangle + \cos\left(\frac{\Omega_0 t_1+\varphi_1+\varphi_2}{2}\right)|1\rangle.$$

The population of the ground/bright state $|0\rangle$ is thus

$$\begin{aligned}P(|0\rangle) &= \left[\sin\left(\frac{\Omega_0 t_1+\varphi_1+\varphi_2}{2}\right)\right]^2 \\ &= \frac{1}{2}\left[1-\cos\left(\Omega_0 t_1+\varphi_1+\varphi_2\right)\right].\end{aligned}$$

Clearly, this corresponds to a Ramsey-fringe pattern, which can be Fourier-transformed to obtain the spectrum (a single line at Ω_0 in this case).

2.2. *Spin $S = 1$ system*

The NV-centre in diamond is a electron spin $S = 1$ system. In this section, we neglect the nuclear spins and write the relevant Hamiltonian

$$\mathcal{H} = DS_z^2 + \Omega_0 S_z. \tag{1}$$

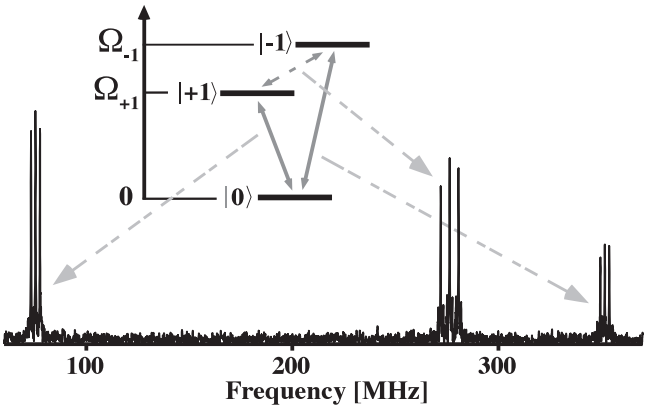

Figure 3. Relevant three-level system of the $S = 1$ electron spin, together with an experimental spectrum. The full arrows indicate allowed magnetic dipole transitions. For experimental conditions see section 2.3.

Here, $D = 2.8$ GHz is the zero-field splitting and Ω_0 the Larmor frequency due to the interaction with the magnetic field. Figure 3 shows the resulting level structure, together with the allowed magnetic dipole transitions, marked by arrows. The dotted arrows assign the transitions to the corresponding lines of the measured spectrum. The transitions show an additional splitting which is due to the hyperfine coupling to the ^{14}N nuclear spin. We write $|m_S\rangle$ for the eigenstates of the Hamiltonian, where m_S is the eigenvalue of S_z.

In the following, we assume that the Rabi frequency is small compared with the frequency separation of the relevant transitions. We therefore can assume that the microwave field drives only one transition at a time [21–23]. If we scan from low to high frequency, we first excite the transition $|0\rangle \leftrightarrow |+1\rangle$ in the system shown in figure 3. Starting from the initial state $\Psi_0 = |0\rangle$, the first passage through resonance converts it into

$$\begin{aligned}\Psi_1 &= U_{zy}(\varphi, \theta)\,|0\rangle \\ &= \mathrm{e}^{\mathrm{i}\varphi/2}\cos\frac{\theta}{2}\,|0\rangle - \mathrm{e}^{-\mathrm{i}\varphi/2}\sin\frac{\theta}{2}\,|+1\rangle\,,\end{aligned}$$

where θ is the effective flip-angle of the pulse. Passing through the second resonance, we obtain

$$\begin{aligned}\Psi_2 &= U_{zy}(\varphi, \theta)\,\Psi_1 \\ &= -\sin\frac{\theta}{2}\cos\frac{\theta}{2}\,|-1\rangle - \mathrm{e}^{-\mathrm{i}\varphi/2}\sin\frac{\theta}{2}\,|+1\rangle + \mathrm{e}^{\mathrm{i}\varphi}\cos^2\frac{\theta}{2}\,|0\rangle\,.\end{aligned}$$

Here, we have assumed that the effect of the pulse on both transitions is the same. This is a good approximation if the scan rate and the transition strengths are the same.

During the subsequent free evolution period, the system evolves to

$$\begin{aligned}\Psi_3 &= U_z(t_1)\,\Psi_2 \\ &= -\mathrm{e}^{-\mathrm{i}(\Omega_{-1}t_1)}\sin\frac{\theta}{2}\cos\frac{\theta}{2}\,|-1\rangle - \mathrm{e}^{-\mathrm{i}(\Omega_{+1}t_1+\varphi/2)}\sin\frac{\theta}{2}\,|+1\rangle + \mathrm{e}^{\mathrm{i}\varphi}\cos^2\frac{\theta}{2}\,|0\rangle\,,\end{aligned}$$

with $\Omega_{\pm 1} = D \mp \Omega_0$ representing the resonance frequencies of the two transitions.

This free precession period is terminated by the readout pulse, which is identical to the excitation pulse (apart from an overall phase). It converts part of the coherences back to

populations:

$$\begin{aligned}\Psi_4 &= U_{yz}(\theta,\varphi)\,\Psi_3 \\ &= B_{-1}\,|-1\rangle + B_{+1}\,|+1\rangle + \left[-A_1(\mathrm{e}^{-\mathrm{i}(\Omega_{-1}t_1+\frac{\varphi}{2})} + \mathrm{e}^{-\mathrm{i}\left(\Omega_{+1}t_1+\frac{\varphi}{2}\right)}) + A_2\,\mathrm{e}^{\mathrm{i}2\varphi}\right]|0\rangle\,.\end{aligned}$$

The coefficients B_{-1} and B_{+1} are not given here since we are interested only in the population $P_0 = P(|0\rangle)$ of the bright state $|0\rangle$:

$$\begin{aligned}P_0 &= \left|A_1(\mathrm{e}^{-\mathrm{i}\left(\Omega_{-1}t_1+\frac{\varphi}{2}\right)} + \mathrm{e}^{-\mathrm{i}\left(\Omega_{+1}t_1+\frac{\varphi}{2}\right)}) + A_2\,\mathrm{e}^{\mathrm{i}2\varphi}\right|^2 \\ &= 2A_1^2 + A_2^2 + 2A_1^2\cos\left(\left[\Omega_{+1}-\Omega_{-1}\right]t_1\right) \\ &\quad + 2A_1A_2\left[\cos\left(\Omega_{+1}t_1+\frac{5\varphi}{2}\right)+\cos\left(\Omega_{-1}t_1+\frac{5\varphi}{2}\right)\right],\end{aligned}$$

with the amplitudes

$$A_1 = \sin^2\frac{\theta}{2}\cos\frac{\theta}{2}, \qquad A_2 = \cos^4\frac{\theta}{2}.$$

The first term in this expression is a constant offset. The second term oscillates at the frequency $2\Omega_0 = \Omega_{-1} - \Omega_{+1}$ of the $|-1\rangle \leftrightarrow |+1\rangle$ transition, while the third term contains the two single quantum transition frequencies. Fourier transformation of this will therefore yield a spectrum with the two allowed single quantum transition and the 'forbidden' double quantum transition frequency, as shown in figure 3. Note that the frequencies in the figure are not the true resonance frequencies. The relation between the apparent and the real frequencies will be discussed in the following section.

2.3. Adiabatic condition

Adiabatic pulses can be used to invert the populations of two states (see e.g. [24]). Here, we use chirped pulses in the non-adiabatic regime to create coherences of many transitions distributed over a broad frequency range. The adiabaticity of a scan can be quantified by the adiabaticity parameter [25]

$$Q(t) = \frac{\omega_{\mathrm{eff}}(t)}{|\mathrm{d}\theta/\mathrm{d}t|}.$$

Here, $\omega_{\mathrm{eff}}(t)$ is the effective magnetic field in the frame rotating with the frequency of the microwave field and $\mathrm{d}\theta/\mathrm{d}t$ indicates the rate of change of the instantaneous eigenstates. Close to resonance, $\omega_{\mathrm{eff}}(t)$ is minimal and equal to the Rabi frequency while $\mathrm{d}\theta/\mathrm{d}t$ reaches a maximum. Hence the adiabaticity factor becomes minimal and can be written as $Q_{\min} = 2\pi\,\nu_1^2 t_{\mathrm{p}}/\Delta f$ [26]. ν_1 is the Rabi frequency, t_{p} the duration of the chirp and Δf the chirp bandwidth. An adiabatic transfer is achieved if $Q_{\min} \gg 1$. The condition for an adiabatic transfer is thus that the rate $\mathrm{d}\theta/\mathrm{d}t$ at which the eigenstates change be small compared to the Rabi frequency ν_1. In our experiments, the transfer must be diabatic, which can be achieved by choosing $\mathrm{d}\theta/\mathrm{d}t > \nu_1$. In our experiments we used Rabi frequencies <30 MHz, pulse durations of 50–120 ns and chirp bandwidths of 250–500 MHz. The maximal value of the adiabaticity parameter used in the measurements was $Q_{\min} < 0.5$. This underlines that the excitations within our experiments were non-adiabatic.

3. Experimental results

In this section we give a short introduction into the experimental procedure and the samples used. Then we present experimental results that demonstrate how the experimental parameters have to be chosen to optimize the information content of the resulting spectra. In addition, we present experimental data from a system that requires a large excitation bandwidth and contains a large number of resonance lines.

3.1. Setup and samples

The experiments were performed with a home-built confocal microscope. A diode-pumped solid-state laser with an emission wavelength of 532 nm was used. The CW laser beam was sent through an acousto-optical modulator to generate laser pulses for excitation and readout. We used an oil immersion microscope objective (with NA = 1.4) mounted on a nano-positioning system to focus the laser light to single NV-centres. The microscope objective also collects light emitted by the NV-centres during readout. For electronic excitation we used a setup consisting of a microwave synthesizer and an arbitrary waveform generator, which were connected to a mixer and up-converted. Here the synthesizer was used as local oscillator and the arbitrary waveform generator, which had a sampling frequency of 4 GS s^{-1}, delivered the intermediate frequency. We were able to control the phase as well as the frequency of the up-converted signal by changing the phase and the frequency of the arbitrary waveform generator. The controllable frequency bandwidth was <2 GHz. The microwaves were guided through a Cu wire mounted on the surface of the diamond. The maximal excitation power was 8 W. We used a permanent magnet to apply a magnetic field to the sample. Unless otherwise mentioned, the orientation of the magnetic field with respect to the axis of the NV centre was not known.

The experiments were carried out as follows: for each point of t_1 the frequency of the pulse was swept from ω_{start} up to the final frequency $\omega_{\text{start}} + \omega_{\text{bdw}}$. A free evolution period of duration t_1 followed the first microwave-pulse. The second pulse was identical to the first up to a phase as discussed in section 3.2. As in conventional Ramsey experiments the time increment of the free evolution period t_1 defines the detection bandwidth and the total duration of the free evolution respectively the maximal value of t_1 defines the spectral resolution. To avoid aliasing effects, we chose the chirp and detection bandwidth equal. The measured time-domain signal was Fourier transformed to recover the spectrum.

We applied the chirped Ramsey sequence shown in figure 2 to two different diamond samples both of type IIa. One is a ^{12}C enriched (concentration of 99.995%) diamond with a relaxation time of $T_2^* > 200\,\mu$s the other a natural abundance diamond with $T_2^* \approx 1\,\mu$s. For the enriched sample the relaxation time was determined by a conventional Ramsey measurement for the natural abundance T_2^* was taken from the chirped measurement.

The enriched sample is a diamond single crystal grown at 5.5 GPa and 1400 °C from Co–Ti–Cu alloy by using a temperature gradient method. As a solid carbon source, polycrystalline diamond plates synthesized by chemical vapour deposition utilizing ^{12}C enriched methane were used [27]. Secondary ion mass spectrometry analysis has shown that typically a ^{12}C concentration of 99.995% in the grown crystals was achieved. The crystal was irradiated at room temperature with 2 MeV electrons and a total flux intensity of 10^{11} cm^{-2}. Subsequently it was annealed at 1000 °C for 2 h in vacuum.

We first present measurements of the enriched sample to illustrate different features of this experiment, in particular how the phases of the excitation pulses affect the observed frequency and phase of the different types of resonance lines. Since we discuss Fourier transformed time-domain signals of photon counts, we use arbitrary units and omit the y-axes in the spectra presented in the following. The pulse durations used in our experiments were chosen with respect to a series of measurements of different pulse lengths which were done for one of the NV-centres of the enriched sample. We chose the pulse duration that yielded the maximum signal for single as well as double quantum coherence. For the other NV-centres the parameters were chosen accordingly to gain similar values for the adiabaticity factor $Q_{\min}$.

In the experiments, we are not interested in the dc component $2A_1^2 + A_2^2$, which we omit in the following. We now compare experiments where we change the phase of the second pulse with respect to that of the first one by an angle α. The resulting signal is then

$$s = 2A_1^2 \cos\left(\left[\Omega_{+1} - \Omega_{-1}\right] t_1\right) + 2A_1 A_2 \left[\sin\left(\Omega_{-1} t_1 + \frac{5}{2}\varphi - \alpha\right) + \sin\left(\Omega_{+1} t_1 + \frac{5}{2}\varphi - \alpha\right)\right]. \quad (2)$$

In the experiments, we use this additional phase for two purposes: we increment it linearly with the free precession period t_1 to shift the effective precession frequency, and we use it to distinguish the double quantum transition, which does not depend on α, from the single quantum transitions.

Looking first at the linear phase increments, we set $\alpha = \omega_0 t_1$. The resulting signal is then

$$s_1 = 2A_1^2 \cos\left(\left[\Omega_{+1} - \Omega_{-1}\right] t_1\right) + 2A_1 A_2 \left[\sin\left(\left(\Omega_{-1} - \omega_0\right) t_1 + \frac{5}{2}\varphi\right) + \sin\left(\left(\Omega_{+1} - \omega_0\right) t_1 + \frac{5}{2}\varphi\right)\right].$$

We therefore expect that the single quantum transitions appear shifted to the frequencies $(\Omega_{\pm 1} - \omega_0)$, while the double quantum transition remains at the natural frequency $2\Omega_0 = \Omega_{+1} - \Omega_{-1}$. This is clearly borne out in figure 4, where we compare spectra obtained with the same excitation scheme, but different reference frequencies. The three groups of lines appear centred around $\Omega_{+1} - \omega_0$, $2\Omega_0 = \Omega_{+1} - \Omega_{-1}$, and $\Omega_{-1} - \omega_0$. For these experiments, we chose ω_0 such that the resulting frequencies fall into a frequency window that is easily accessible. In the case of the spectra shown here, we incremented t_1 by 2 ns between scans, which yields, according to the Nyquist theorem a 250 MHz frequency window. The maximum value of t_1 was 5 μs. The Rabi frequencies of the single quantum transitions were 10.5 MHz (leftmost triplet) and 11.1 MHz (rightmost triplet). The number of accumulations was 2×10^5. The data were recorded in the same magnetic field, which splits the $|m_s = \pm 1\rangle$ lines by 146 MHz. All measurements were done with frequency chirps starting at 2770 MHz and the pulse lengths were $\tau_p = 120$ ns. It is clearly seen that the single quantum transitions are shifted in the opposite direction from the reference frequency, while the double quantum transitions (at 146 MHz) are not affected by the detuning.

3.2. Phase shifts

Instead of incrementing the phase proportionally with t_1, we can also compare two spectra with different constant phase shifts of the readout pulse. The two traces of figure 5(b) show an example: the spectra were obtained with phase shifts of 0 and π between the two pulses; only

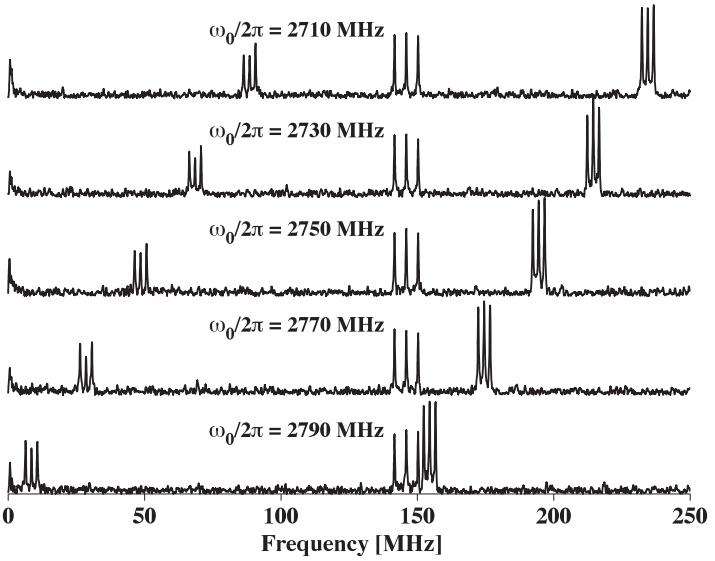

Figure 4. Ramsey spectra measured with different reference frequencies. The actual transition frequencies are: $\Omega_{+1}/2\pi = 2798.5\,\text{MHz}$, $\Omega_{-1}/2\pi = 2944.5\,\text{MHz}$ and $2\Omega_0/2\pi = 146\,\text{MHz}$. The reference frequencies are given in the figure. For all spectra, the start frequency of the chirp was $\omega_{\text{start}} = 2770\,\text{MHz}$ and the chirp bandwidth $\omega_{\text{bdw}} = 250\,\text{MHz}$.

expanded regions of the full spectrum shown in figure 5(a) are shown. These data were recorded with a different NV-centre in a higher magnetic field strength. The Rabi frequencies of the single quantum transitions were 27.3 MHz (leftmost triplet) and 21.7 MHz (rightmost triplet). The number of accumulations was 4×10^5. The differences in intensity of the single quantum coherences might be due to a frequency dependence of the pulse power. The chirp bandwidth was 500 MHz and the pulse duration $\tau_p = 50\,\text{ns}$. The detection bandwidth was 500 MHz and the maximum value of t_1 was 5 μs.

According to equation (2), we expect that the phase of the single quantum transitions $|0\rangle \leftrightarrow |\pm 1\rangle$ should change with α, while the double quantum transition $|+1\rangle \leftrightarrow |-1\rangle$ should not change. Inspection of the experimental data shows that the spectral lines close to 60 and 375 MHz are inverted between the two spectra, while the signals close to 315 MHz do not change. We therefore interpret the outer lines as single quantum transitions, the inner ones as double quantum transitions. This assignment is also consistent with the splittings due to the hyperfine interaction with the ^{14}N nuclear spin, which is 2.15 MHz for the single quantum transitions and 4.3 MHz for the double quantum transition.

Using this phase dependence, we can also separate the two types of transitions by calculating the sum and difference of the two spectra. According to equation (2), the difference of the two spectra should be

$$s_{\alpha=0^\circ} - s_{\alpha=180^\circ} = 4A_1A_2\left[\sin\left(\Omega_{-1}t_1 + \frac{5}{2}\varphi\right) + \sin\left(\Omega_{+1}t_1 + \frac{5}{2}\varphi\right)\right], \tag{3}$$

and the sum

$$s_{\alpha=0^\circ} + s_{\alpha=180^\circ} = 4A_1^2\cos\left(2\Omega_0 t_1\right). \tag{4}$$

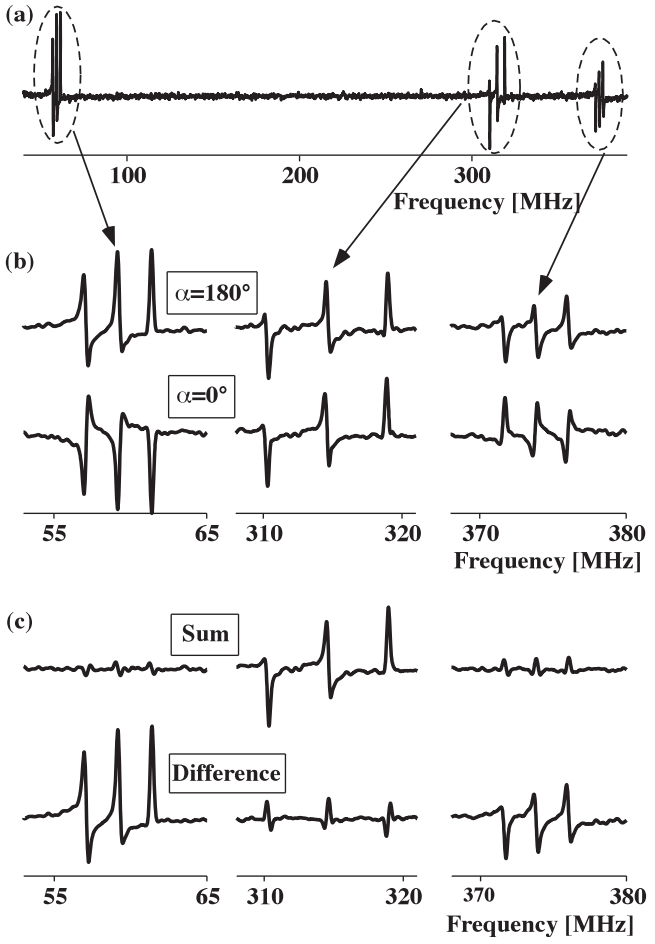

Figure 5. Phase-sensitive spectra of two chirped Ramsey measurements. (a) Full spectrum. (b) Real parts of spectra obtained with phase shifts $\alpha = 180^\circ$ (top) and $\alpha = 0^\circ$ (bottom). (c) Sum (top) and difference (bottom) of the spectra in (b).

The lower part of figure 5 shows the result of this operation: the sum (upper trace) contains mostly the double quantum signals, while the difference is dominated by the single quantum transitions which corresponds to the results of equations (3) and (4). The incomplete suppression of the other signals can be attributed to instabilities in the experimental setup, which result in thermal frequency shifts and changing amplitudes.

3.3. B-field dependence

Figure 6 shows spectra of the ^{12}C enriched crystal for different magnetic field strengths. For these measurements the reference frequency was $\omega_0 = 2670.8$ MHz. The start frequency of the chirp was $\omega_{\text{start}} = 2650.8$ MHz, the chirp bandwidth $\omega_{\text{bdw}} = 500$ MHz and the pulse duration $\tau_p = 50$ ns. The sampling interval of 1 ns results in a detection bandwidth of 500 MHz and maximum value of t_1 of 5 μs yields a digital frequency resolution of 100 kHz.

In each spectrum of the figure, we list the splitting between the single quantum transitions, which corresponds to the magnetic field component along the symmetry axis of the centre, measured in frequency units. The outer triplets correspond to the single quantum

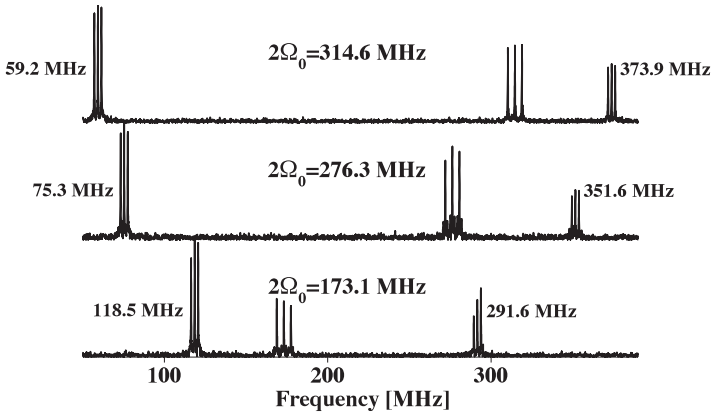

Figure 6. Absolute value spectra for different magnetic field strengths. $2\Omega_0$ corresponds to the separation of the $|+1\rangle$, $|-1\rangle$ levels and therefore to the separation between the two single quantum transitions and to the centre frequency of the double quantum transition (inner line of the triplet). The frequency values give the positions of the central line of the respective triplet. The Rabi frequencies and number of accumulations are identical to those in section 3.2.

transitions ($|0\rangle \leftrightarrow |\pm 1\rangle$), the inner lines to the double quantum transition ($|+1\rangle \leftrightarrow |-1\rangle$). With increasing magnetic field strength, the splitting between the single quantum transitions increases proportionally and is always equal to the frequency of the double quantum transition. The frequencies of the single quantum transitions do not change symmetrically. The mean values of the central lines of the single quantum transitions are: $(\Omega_+ + \Omega_-)/2 = 205$, 213 and 216 MHz. This variation is due to non-secular terms of the Zeeman interaction (i.e. $S_x B_x + S_y B_y$) which we have neglected in the Hamiltonian in equation (1).

3.4. Multi-line broadband spectrum

The chirped excitation scheme is particularly useful when the spectra cover a broad frequency range with many resonance lines. Such a situation exists in NV-centres with a ^{13}C nuclear spin in the first coordination shell.

Figure 7 shows the spectrum of such a centre. In this particular centre, the electron spin is coupled to a nearest-neighbour ^{13}C nuclear spin with a hyperfine coupling constant $A_\parallel \approx 126.5$ MHz as well as to an additional ^{13}C with a coupling constant of $A_\parallel \approx 6.55$ MHz. For this measurement we used a type IIa natural abundance diamond and applied a magnetic field of $\approx$9 G. The field was not aligned and had an angle of $\approx 65^\circ$ with respect to the symmetry axis of the NV-centre, which corresponded to a projected field strength of 3.7 G. The chirp bandwidth was $\omega_{\mathrm{bdw}} = 250$ MHz, starting from $\omega_{\mathrm{start}} = 2750.3$ MHz and the pulse-duration was $\tau_{\mathrm{p}} = 60$ ns. The detection bandwidth was 250 MHz and the maximum value of $t_1 = 3\,\mu$s. The number of accumulations was 2.36×10^7.

The top graph of figure 7 shows the absolute value of a chirped Ramsey spectrum. The centre graph shows the sum and the lower the difference of two phase-shifted spectra, which correspond to the double- and single quantum transitions, respectively. The line at 126.5 MHz in (b) is a zero-quantum transition. Its transition frequency matches the hyperfine coupling

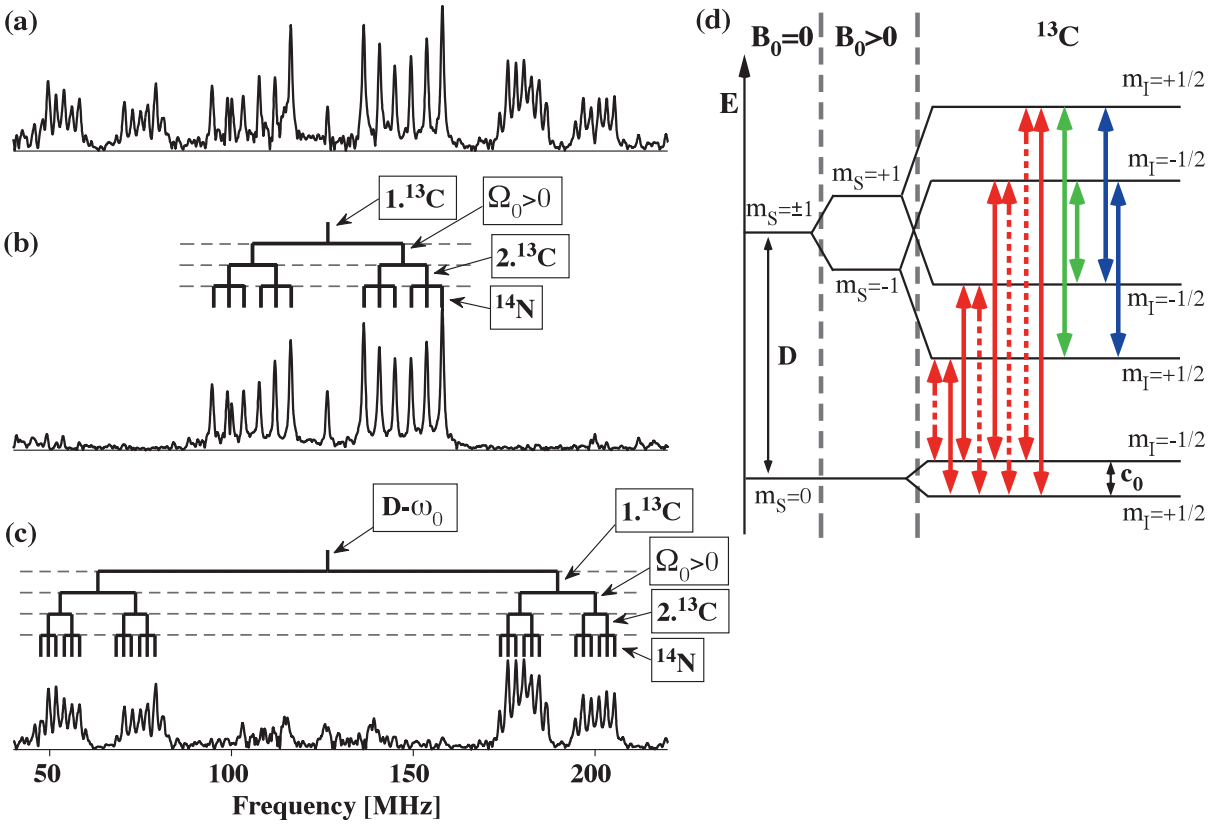

Figure 7. Spectra of NV-centre in natural abundance diamond with two adjacent ^{13}C nuclear spins. One strongly coupled with $A_{\parallel} \approx 126.5$ MHz (nearest-neighbour) and one with $A_{\parallel} \approx 6.55$ MHz [15]. $\Omega_0 \approx 10$ MHz is the Zeeman interaction, D the zero-field splitting and ω_0 the reference frequency. (a) Absolute value spectrum. (b) Sum and (c) difference of the spectra obtained with phase shifts $\alpha = 0$ and 180°. (d) Energy level scheme of the NV electron spin coupled to a nearest-neighbour ^{13}C within a small external magnetic field $B_0 > 0$. c_0 indicates a splitting of the electron spin ground state due to the coupling to the ^{13}C nuclear spin. For the sake of simplicity we have omitted the couplings to the ^{14}N nuclear spin and the additional ^{13}C.

constant of the nearest-neighbour ^{13}C. In the spectra, we also indicate how the spectral lines can be assigned to transitions of the electron spin with different configurations of the three coupled nuclear spins. If we consider only the Hamiltonian of equation (1) for the electron spin and the hyperfine interactions with the nuclear spins, the single quantum spectrum (bottom of figure 7) should consist of four groups of six lines. In the experimental spectrum, the four groups contain more than six lines. This difference can be attributed to the splitting of the $|m_S = 0\rangle$ ground state due to the interaction with the transverse components of the magnetic field and the non-secular hyperfine interaction. Figure 7(d) shows a level scheme, which takes into account that the non-secular terms of the hyperfine interaction lift the degeneracy of the two spin states of the ^{13}C nuclear spin associated with the $|m_S = 0\rangle$ state [28]. The solid red arrows indicate allowed single quantum transitions and the dashed red arrows indicate 'forbidden'

single quantum transitions, where both, the nuclear *and* electron spin flip. The green arrows indicate double quantum transitions and the blue arrows zero quantum transitions.

As a result of the nonsecular terms in the hyperfine interaction, the electronic and nuclear spin degrees of freedom do not factorize and a microwave field can drive transitions between any pair of states whose energy difference matches the resonance condition, including 'forbidden' transitions. Throughout the scan, the resonance condition becomes fulfilled for different connected transitions and the field thereby generates also coherences between states whose energy difference does not match the microwave frequency. As discussed in section 2.2, this leads to the excitation of double quantum coherence and in a similar way to the excitation of zero quantum coherence between the $|m_S = \pm 1, \uparrow\rangle$ and $|m_S = \pm 1, \downarrow\rangle$ states (see figure 7(b)).

4. Conclusions

We have introduced a new experimental technique for measuring broad spectra of single electron spins. This approach does not require high microwave power. The precession frequency of the spins is measured in the absence of microwave irradiation, in the form of Ramsey fringes, which results in high resolution spectra. The resulting spectra contain not only the dipole-allowed single quantum transitions, but also multiple quantum transitions that can only be excited by multiple absorption/emission processes. This technique is particularly useful in the case of electron spins coupled to multiple nuclear spins. Such clusters of spins may be useful tools for quantum computing applications [11–14]. We have demonstrated the technique on the example of single electron spins in the diamond NV-centre, but the same approach should also be applicable to other systems, where the excitation bandwidth can be sufficiently large.

Acknowledgments

This work was supported by the Deutsche Forschungsgesellschaft through grant no. Su 192/27-1 (FOR 1482).

References

[1] Jelezko F and Wrachtrup J 2006 Single defect centres in diamond: a review *Phys. Status Solidi* a **203** 3207–25
[2] Maze J R *et al* 2008 Nanoscale magnetic sensing with an individual electronic spin in diamond *Nature* **455** 644–7
[3] Maletinsky P, Hong S, Grinolds M S, Hausmann B, Lukin M D, Walsworth R L, Loncar M and Yacoby A 2012 A robust scanning diamond sensor for nanoscale imaging with single nitrogen–vacancy centres *Nature Nano* **7** 320–4
[4] Rondin L, Tetienne J-P, Spinicelli P, Dal Savio C, Karrai K, Dantelle G, Thiaville A, Rohart S, Roch J-F and Jacques V 2012 Nanoscale magnetic field mapping with a single spin scanning probe magnetometer *Appl. Phys. Lett.* **100** 153118
[5] Dolde F *et al* 2011 Electric-field sensing using single diamond spins *Nature Phys.* **7** 459–63
[6] Acosta V M, Bauch E, Ledbetter M P, Waxman A, Bouchard L-S and Budker D 2010 Temperature dependence of the nitrogen–vacancy magnetic resonance in diamond *Phys. Rev. Lett.* **104** 070801
[7] Toyli D M, Christle D J, Alkauskas A, Buckley B B, Van de Walle C G and Awschalom D D 2012 Measurement and control of single nitrogen–vacancy center spins above 600 k *Phys. Rev. X* **2** 031001
[8] Kolkowitz S, Unterreithmeier Q P, Bennett S D and Lukin M D 2012 Sensing distant nuclear spins with a single electron spin *Phys. Rev. Lett.* **109** 137601

[9] Taminiau T H, Wagenaar J J T, van der Sar T, Jelezko F, Dobrovitski V V and Hanson R 2012 Detection and control of individual nuclear spins using a weakly coupled electron spin *Phys. Rev. Lett.* **109** 137602
[10] Zhao N *et al* 2012 Sensing single remote nuclear spins *Nature Nano* **7** 657–62
[11] Gurudev Dutt M V, Childress L, Jiang L, Togan E, Maze J, Jelezko F, Zibrov A S, Hemmer P R and Lukin M D 2007 Quantum register based on individual electronic and nuclear spin qubits in diamond *Science* **316** 1312–6
[12] Cappellaro P, Jiang L, Hodges J S and Lukin M D 2009 Coherence and control of quantum registers based on electronic spin in a nuclear spin bath *Phys. Rev. Lett.* **102** 210502
[13] Mizuochi N *et al* 2009 Coherence of single spins coupled to a nuclear spin bath of varying density *Phys. Rev.* B **80** 041201
[14] Neumann P *et al* 2010 Quantum register based on coupled electron spins in a room-temperature solid *Nature Phys.* **6** 249–53
[15] Smeltzer B, Childress L and Gali A 2011 ^{13}C hyperfine interactions in the nitrogen–vacancy centre in diamond *New J. Phys.* **13** 025021
[16] Dréau A, Maze J-R, Lesik M, Roch J-F and Jacques V 2012 High-resolution spectroscopy of single NV defects coupled with nearby ^{13}C nuclear spins in diamond *Phys. Rev.* B **85** 134107
[17] Felton S, Edmonds A M, Newton M E, Martineau P M, Fisher D, Twitchen D J and Baker J M 2009 Hyperfine interaction in the ground state of the negatively charged nitrogen vacancy center in diamond *Phys. Rev.* B **79** 075203
[18] Dréau A, Lesik M, Rondin L, Spinicelli P, Arcizet O, Roch J-F and Jacques V 2011 Avoiding power broadening in optically detected magnetic resonance of single NV defects for enhanced dc magnetic field sensitivity *Phys. Rev.* B **84** 195204
[19] Ramsey N F 1950 A molecular beam resonance method with separated oscillating fields *Phys. Rev.* **78** 695–9
[20] Vion D, Aassime A, Cottet A, Joyez P, Pothier H, Urbina C, Esteve D and Devoret M H 2003 Rabi oscillations, Ramsey fringes and spin echoes in an electrical circuit *Fortschr. Phys.* **51** 462–8
[21] Ferretti J A and Ernst R R 1976 Interference effects in NMR correlation spectroscopy of coupled spin systems *J. Chem. Phys.* **65** 4283–93
[22] Burghardt I, Bohlen J-M and Bodenhausen G 1990 Broadband multiple-quantum nuclear magnetic resonance with frequency-modulated 'chirp' pulses: applications to pairs of scalar-coupled spin $i = 1/2$ nuclei *J. Chem. Phys.* **93** 7687–97
[23] Jeschke G and Schweiger A 1995 Time-domain chirp electron nuclear double resonance spectroscopy in one and two dimensions *J. Chem. Phys.* **103** 8329–37
[24] Fuchs G D, Dobrovitski V V, Toyli D M, Heremans F J and Awschalom D D 2009 Gigahertz dynamics of a strongly driven single quantum spin *Science* **326** 1520–2
[25] Messiah A 1970 *Quantum Mechanics* (Amsterdam: North-Holland)
[26] Doll A, Pribitzer S, Tschaggelar R and Jeschke G 2013 Adiabatic and fast passage ultra-wideband inversion in pulsed EPR *J. Magn. Res.* **230** 27–39
[27] Teraji T, Taniguchi T, Koizumi S, Watanabe K, Liao M, Koide Y and Isoya J 2012 Chemical vapor deposition of ^{12}C isotopically enriched polycrystalline diamond *Japan J. Appl. Phys.* **51** 090104
[28] Shim J. *et al* 2013 in preparation

Broadband excitation by chirped pulses: application to single electron spins in diamond

2013 New J. Phys. 15 033027

(http://iopscience.iop.org/1367-2630/15/3/033027)